Applied Catalysis B: Environmental 163 (2015) 150–155

Contents lists available at ScienceDirect

Applied Catalysis B: Environmental

journal homepage: www.elsevier.com/locate/apcatb

Full Length Article

Mesoporous WO_3 photocatalyst for the partial oxidation of methane to methanol using electron scavengers

Katherine Villa[a,*], Sebastián Murcia-López[a], Teresa Andreu[a,*,1], Joan Ramón Morante[a,b]

[a] Catalonia Institute for Energy research (IREC), Jardins de les Dones de Negre 1, 08930 Sant Adrià de Besòs, Spain
[b] Department of Electronics, University of Barcelona (UB), Marti i Franquès 1, 08028 Barcelona, Spain

ARTICLE INFO

Article history:
Received 3 June 2014
Received in revised form 21 July 2014
Accepted 25 July 2014
Available online 12 August 2014

Keywords:
Mesoporous WO_3
Photocatalysis
CH_4 conversion
Methanol

ABSTRACT

Mesoporous WO_3 was synthesized by replicating technique using ordered mesoporous silica KIT-6 as the template. The obtained material exhibits high surface area (151 $m^2\,g^{-1}$) and porous structure. The photocatalytic conversion of methane into methanol from an aqueous suspension containing mesoporous WO_3 was studied, as well as the effect of the addition of electron scavengers (Fe^{3+}, Cu^{2+}, Ag^+) and H_2O_2 species. In the presence of Fe^{3+} ions the production of methanol was about two and a half times higher than that of pure mesoporous WO_3, which was principally attributed to the largely improved electron-hole separation in this system. However, the CO_2 generation rates were also increased, mainly in the presence of Ag^+ ions. It was also corroborated that extra hydroxyl radicals in the aqueous medium do not improve the generation of methanol but a noticeable increase in the formation of ethane was evidenced. This suggests that only a higher availability of $HO^{\bullet}$'s adsorbed on the catalyst can enhance the performance of methanol generation in the photocatalytic process.

1. Introduction

Methane is a highly stable hydrocarbon with a wide distribution in nature. Moreover, it is the principal component of natural gas (about 75–90%). Due to its abundance, this gas could provide a new alternative in the field of fuels and chemicals [1]. For instance, the methane conversion into methanol is a good alternative to obtain a liquid compound that can be used as starting material to synthesize a variety of chemicals such as formaldehyde, acetic acid, methyl *t*-butyl ether, etc. Also, methanol is considered a much more efficient fuel than petroleum-based ones [2,3].

Photocatalysis is one of the processes that allow this methane conversion under mild conditions, by using an appropriate catalyst and light. In this sense, this technique can be considered a green alternative for performing selective oxidations in a wide range of applications [4]. Among the candidate materials that have been examined as possible photocatalysts, tungsten oxide (WO_3) is one of the most promising, due to its high chemical stability in aqueous solution under acidic conditions, non-toxicity, and moderate oxidizing power. For example, Gondal et al. found that, in comparison to TiO_2 and NiO, the WO_3 showed the largest conversion of methane to methanol [5]. On the other hand, the addition of chemical additives to improve the performance of WO_3 in this photocatalytic reaction has also been reported. Taylor and Noceti showed that the addition of H_2O_2 improved the generation of methanol, as this species can be a source of hydroxyl radicals, which are an important intermediate that contributes to the CH_3OH formation [6]. In contrast, Gondal et al. evidenced that hydrogen peroxide has no influence in enhancing the production yield of methanol but the addition of Fe^{3+} can help to maintain the production of methanol over the reaction (batch type) [7].

Recently, there has been a growing interest in ordered mesostructures of metal oxides due to their properties and wide potential applications. This kind of materials exhibit a large surface area that improves the adsorption of reactant molecules [8] and the ordered mesopore channels facilitate fast intraparticle molecular transfer, resulting in a decrease of charge recombination and thus, a higher photoactivity. Ordered mesoporous WO_3 has been widely studied for sensor applications [9,10,11], but limited studies have been performed for photocatalytic reactions [12,13,14]. To the best of our knowledge, there is no report on the application of ordered mesoporous WO_3 toward methane conversion by photocatalysis. Hence, in this work we investigated the partial photocatalytic oxidation of methane into methanol using an ordered mesoporous WO_3 that exhibits high crystallinity. Although

* Corresponding authors. Tel.: +34 933 562 615.
E-mail addresses: kvilla@irec.cat (K. Villa), tandreu@irec.cat (T. Andreu).
[1] Tel.: +34 933 562 615.

http://dx.doi.org/10.1016/j.apcatb.2014.07.055
0926-3373/

prior works have reported the effect of the addition of Fe^{3+} and H_2O_2 on the reaction yield, a more comprehensive study of the efficacy of such systems has been lacking. Thus, the influence of the addition of several chemical additives as Fe^{3+}, Cu^{2+}, Ag^+ and H_2O_2 in the photoactivity and the role of free hydroxyl radicals in the reaction mechanism to produce methanol or ethane was also studied.

2. Experimental

2.1. Reagents

Tetraethyl orthosilicate (TEOS, ≥99.0%), poly(alkylene oxide)-based triblock copolymer Pluronic P-123 ($EO_{20}PO_{70}EO_{20}$, MW = 5.800), $AgNO_3$, $FeCl_3$, Cu_2SO_4 and H_2O_2, were purchased from Sigma–Aldrich. Other chemicals as 1-butanol (99.0%) and phosphotungstic acid hydrate were obtained from Alfa Aesar. Commercial gas mixtures of 500 ppmv of CH_3OH in He, 1% of CO_2 in air and a mixture of hydrocarbons with 250 ppmv of C_2H_6, 100 ppmv of CH_3CH_2OH and 250 ppmv of C_2H_4 were used for GC calibration.

2.2. Sample preparation

KIT-6 mesoporous silica template with cubic *Ia3d* structure was synthesized in acidic conditions using a mixture of Pluronic P-123 and 1-butanol, as reported in literature [15]. Ordered mesoporous WO_3 was prepared as follows: a solution of 5 mmol of phosphotungstic acid hydrate in ethanol was incorporated into 0.75 g of as-prepared KIT-6 silica under stirring. The sample was dried and then calcined for 4 h at 350 °C to decompose the precursors, and then further at 550 °C for 6 h to obtain WO_3 inside the hosting silica. Later, the obtained material was suspended under stirring in a 10 wt% HF solution to remove the KIT-6 silica template. Finally, the mesoporous WO_3 catalyst was separated by centrifugation, washed sequentially with water and ethanol and dried at room temperature.

2.3. Catalyst characterization

The crystal structure and the optical absorption of the catalyst were characterized by XRD and UV–Vis diffuse reflectance spectroscopy, respectively. The detailed procedures are described in the Supporting Information. A Zeiss Auriga FESEM microscope was used to perform scanning microscopy of the sample and TEM images were taken on a Zeiss LIBRA 120 instrument. BET surface area was obtained with a Micromeritics TriStar II apparatus. *In situ* DRIFT spectra were collected on a Bruker Vertex 70 FTIR spectrometer supplied with a diffuse reflectance attachment and with a MCT detector. The catalyst powder weighing approximately 10 mg was then pressed mechanically to obtain a disk. This disk was placed into the diffuse reflectance infrared cell with CaF_2 windows. The sample was firstly cleaned under flow of helium at 150 °C for 24 h. The spectrum was referenced to that of the catalyst at 55 °C before the introduction of feed gases. After this, CH_4 bubbled in water was dosed into cell for one hour. Finally, the sample was irradiated for 2 h. *In situ* absorbance spectra were obtained each minute by collecting 16 scans at 4 cm^{-1} resolution.

2.4. Photocatalytic setup

The photocatalytic partial oxidation of methane was carried out in a photochemical reactor (Ace Glass) of 500 mL volume equipped with gas inlet and outlet. A medium pressure quartz mercury-vapor lamp (immersion-type Ace Glass) inside the reactor was used to provide UVC-visible light irradiation. The reaction temperature was maintained at 55 °C by recirculation of cold water in the outer jacket of the lamp. A mixture of methane (4.5 mL min^{-1}) and helium (17.9 mL min^{-1}) was sparged continuously through the photocatalytic reactor. In order to avoid methanol condensation during the path, a heating tape was wrapped around the tube outlet from the reactor up to the port valve of the gas chromatograph (GC). A six port valve with a 0.5 mL loop was connected to the circuit to allow gas sample injection into GC. In a typical experiment 300 mL of water (milli-Q) containing 0.3 g of WO_3 were placed in the reactor. Prior to illumination, the suspension was magnetically stirred in the dark for 30 min to reach adsorption-desorption equilibrium. After that, the lamp was turned on and gas samples were periodically taken for analysis. Aqueous solutions of Fe^{3+} (2 mM), Cu^{2+} (0.1 mM), Ag^+ (2 mM) and H_2O_2 (2 mM) were used as redox mediators to improve the photocatalytic activity of WO_3. In the case of copper, a lower concentration was used because it has been reported that larger amounts to 0.1 mM might negatively affect the performance [16]. The initial pH of the suspension was adjusted to ~3 with 1 M H_2SO_4.

2.5. Analytical determinations

Detection and quantification of CH_3OH were carried out by using a Shimadzu GC-2010 chromatograph equipped with a capillary column (HP-PLOT Q), a thermal conductivity detector (TCD) and a flame ionization detector (FID). Pure He (99.99999%) was used as carrier gas. A chromatographic ramp reported in literature was chosen [5]. Under these conditions a good separation of the peaks of products can be achieved and water can be effectively removed from the column.

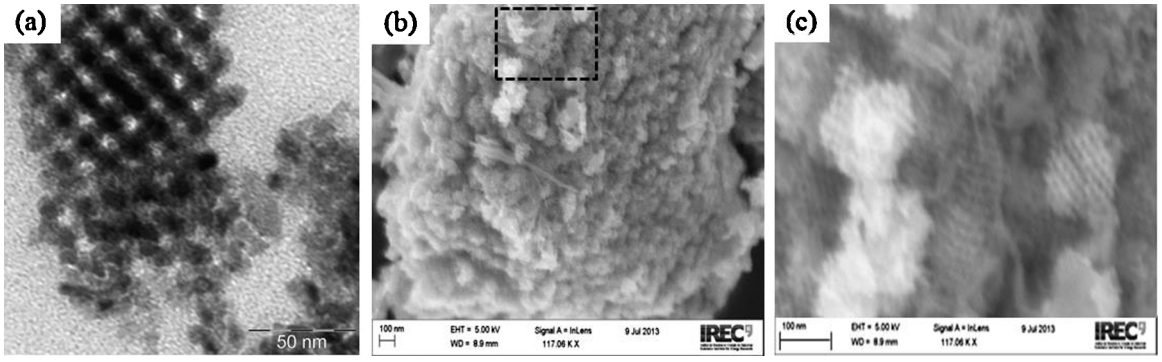

Fig. 1. (a) TEM image of mesoporous WO_3, (b) SEM image of mesoporous WO_3 and (c) magnification of the area marked by the dotted line square in (b).

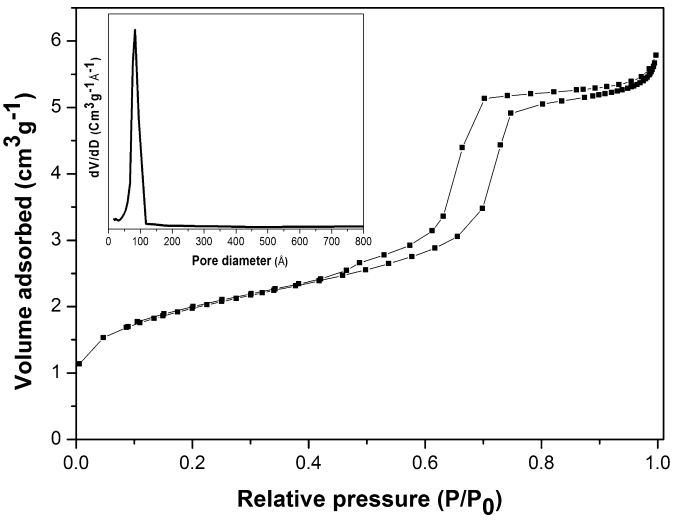

Fig. 2. N_2 adsorption/desorption isotherms and corresponding pore size distribution curves (inset) for mesoporous WO_3.

3. Results and discussion

3.1. Photocatalyst characterization

The XRD pattern of WO_3 is illustrated in Fig. S1 in Supporting Information. All of the diffraction peaks can be indexed to the monoclinic structure of WO_3 (JCPDS Card No. 43-1035). The crystal size was estimated to be 11.7 nm using the Scherrer equation [17]. As can be seen from Fig. 1, the WO_3 prepared consists of a well-ordered structure with irregularly-shaped pores, indicating that the catalyst is a good replica of the KIT-6 silica template.

The nitrogen adsorption and desorption isotherms and pore size distribution curve (inset) of WO_3 are shown in Fig. 2. The isotherm obtained reveals type IV hysteresis loop which is characteristic of mesoporous solids. The BET surface area is 151 $m^2\,g^{-1}$. In addition, the pore size distribution diagram clearly confirms that the pore is in the mesoporous region (87 Å). These results show that the ordered WO_3 synthetized has a large surface area mainly due to the pore connectivity characteristic of porous materials.

The band gap energy (E_g) of the material was calculated from the absorption data by using the Tauc relation [18].

$$\alpha h\nu = A(h\nu - E_g)^m \quad (1)$$

Where $h\nu$ is the photon energy, E_g is the estimated band gap energy and A is a constant. The value of m may be taken as $m = 2$, a characteristic value for the indirect allowed transition, or as $m = 1/2$, a characteristic value for the direct allowed transition. WO_3 is considered an indirect band gap semiconductor [19]; hence, by plotting $(\alpha h\nu)^{1/2}$ versus $h\nu$, the band gap energy can be obtained from the intercept of the tangent to the X axis (see the Supporting Information, Fig. S2). The estimated value is 2.7 eV, which is similar to other values reported in the literature for monoclinic WO_3 (~2.8 eV) [20,21,22].

3.2. Photocatalytic activity for methanol generation

The general photocatalytic reaction can be expressed by the following set of equations. When the WO_3 slurries are irradiated with light energy higher than ~2.7 eV, electron (e^-) and hole (h^+) pairs are generated (Eq. (2)). Then, the photogenerated holes can react with water or hydroxide ions adsorbed on the surface to produce hydroxyl radicals (Eqs. (3) and (4)), which would react with CH_4 to produce methanol as shown in Eqs. (5) and (6).

$$WO_3 \xrightarrow{h\nu} e^-_{CB} + h^+_{VB} \quad (2)$$

$$h^+_{VB} + H_2O_{ads} \rightarrow HO^{\cdot}_{ads} + H^+ \quad (3)$$

$$h^+_{VB} + HO^-_{ads} \rightarrow HO^{\cdot}_{ads} \quad (4)$$

$$CH_4 + HO^{\cdot}_{ads} \rightarrow CH^{\cdot}_3 + H_2O \quad (5)$$

$$CH_3 + H_2O_{ads} \rightarrow CH_3OH + \frac{1}{2}H_2 \quad (6)$$

Additionally, it has been reported that the direct photolysis of water by irradiation with wavelengths ≥ 185 nm also generates hydroxyl radicals (Eq. (7)) [23]. To determine the influence of water on the methane conversion, a blank experiment (in absence of catalyst) was carried out under UVC–visible irradiation. It was found a yield of methanol of 4.9 μmol h^{-1}. This value is almost half of what is produced with the single WO_3.

$$H_2O \xrightarrow{h\nu(\lambda \geq 185\,nm)} 1/2H_2 + HO^{\bullet} \quad (7)$$

On the other hand, hydrogen could also be produced through the reduction of protons by the formed electrons (Eqs. (8) and (9)). However, the conduction band (CB) potential (+0.4 V vs NHE at pH 0) of WO_3 is not negative enough to reduce H^+ to H_2. As a result, these photogenerated electrons react with WO_3 and protons to produce hydrogen tungsten bronze ($H_xW^V{}_xW^{VI}{}_{1-x}O_3$). Consequently, a change in coloration to deep blue is observed after irradiation due to charge transfer from the newly formed W^{5+} to adjacent W^{6+} [24,25]. When the resulting suspension is exposed to air, the original color is recovered, suggesting that W^{5+} is easily oxidized to W^{6+} by oxygen.

$$H^+ + e^-_{CB} \rightarrow H^{\bullet} \quad (8)$$

$$H^{\cdot} + H^{\cdot} \rightarrow H_2 \quad (9)$$

This self-reduction process was confirmed by *in situ* DRIFTS measurements. Fig. 3 shows the DRIFTS spectra obtained when CH_4 (bubbled in water) was passed over WO_3 before and after irradiation. A negative band at 1860 cm^{-1}, which is attributed to W—O and/or W=O vibration modes due to the overtones in monoclinic WO_3 [26,27], resulted from the subtraction of the catalyst spectra from the *in situ* spectra. The peak around 970 cm^{-1} is assigned to some W=O groups [28]. After irradiation, the intensity of the negative peak at 1860 cm^{-1} increases, indicating that these functional groups disappear during reaction along with the peak around 970 cm^{-1}. The observed decrease of intensity of these peaks is induced by the presence of reduced state W^{5+} [29]. Simultaneously, two bands located at 1645 cm^{-1} and 1453 cm^{-1} disappear from the spectra during the reaction, these peaks corresponding to the bending mode of physisorbed water and OH groups strongly bonded to either water molecules or to surface oxygen atoms, respectively [30]. Therefore, the dissociation of water on the surface of WO_3 with optically excited electron–hole pairs provides H atoms that are involved in the formation of the hydrogen tungsten bronze [31,32]. Additionally, new bands appear at 820 and 670 cm^{-1} (Fig. 5b). According to the literature, the band at 820 cm^{-1} represents some of the W—O modes resulting after insertion of protons at the defect sites in the structure [33]. The sharp absorption band at 670 cm^{-1} is assigned to the out of plane deformation W—O—W mode when hydrogen is located at a coplanar square of oxygen atoms [34,35].

In order to avoid the reduction process of WO_3 itself by the photogenerated electrons that involves a gradual loss of photoactivity and the rapid recombination of charge carriers (e^-–h^+), it is essential to capture the electrons during photocatalytic reaction to

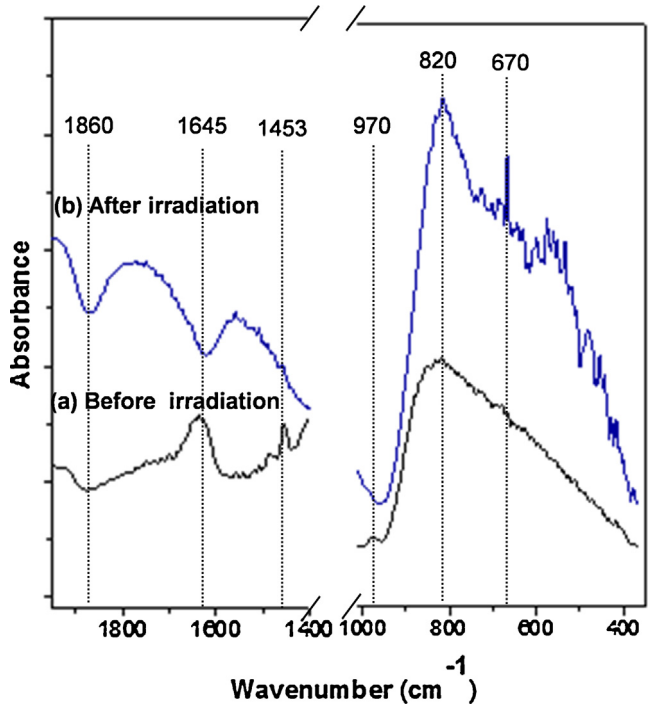

Fig. 3. *In situ* DRIFTS spectra recorded at 55 °C under CH_4 and H_2O flow for (a) WO_3 before irradiation and (b) WO_3 after 2 h of irradiation UV–visible light.

have a higher charge separation and, at the same time, increase the generation of methanol.

The effect of electron scavengers on the production of CH_3OH was examined by the addition of Fe^{3+}, Cu^{2+}, and Ag^{+} in the aqueous suspension. The result is presented in Fig. 4. The presence of Fe^{3+} and Cu^{2+} markedly improves the generation of methanol. These species capture the photogenerated electrons, improving the charge separation that favors the production of $HO^{\bullet}_{ads}$ and thus, a higher amount of CH_3OH is generated. Moreover, no changes in the color of WO_3 were observed after photocatalytic reactions in

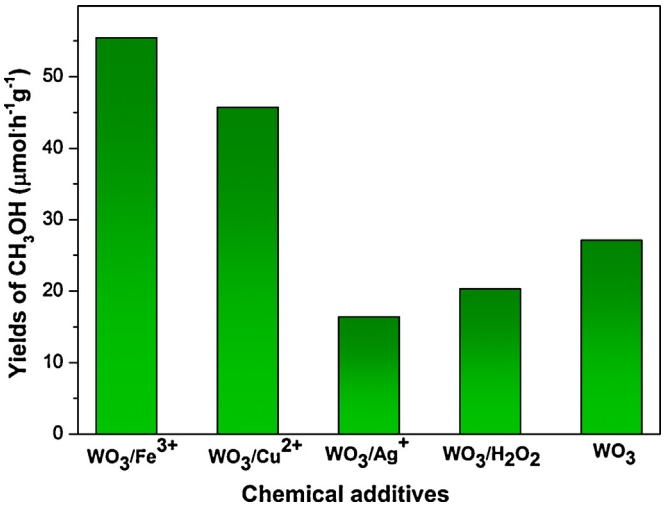

Fig. 4. Yields of CH_3OH in the photocatalytic oxidation of CH_4 in systems of WO_3/Fe^{3+} (2 mM), WO_3/Cu^{2+} (0.1 mM), WO_3/Ag^{+} (2 mM), WO_3/H_2O_2 (2 mM) and WO_3 at ~55 °C under UVC–visible light irradiation. WO_3 dosage is 1 g L^{-1}. Data corresponding to 2 h of irradiation in continuous methane flow of 4.5 mL min^{-1}.

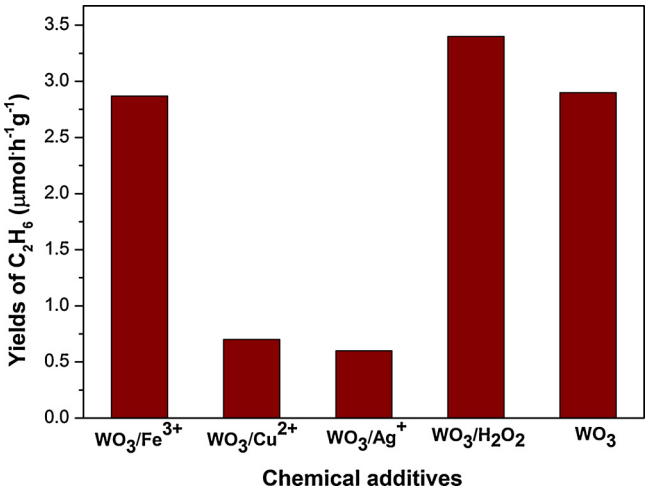

Fig. 5. Yields of C_2H_6 in the photocatalytic oxidation of CH_4 in systems of WO_3/Fe^{3+} (2 mM), WO_3/Cu^{2+} (0.1 mM), WO_3/Ag^{+} (2 mM), WO_3/H_2O_2 (2 mM) and WO_3 at ~55 °C under UVC–visible light irradiation. WO_3 dosage is 1 g L^{-1}. Data corresponding to 2 h of irradiation in continuous methane flow of 4.5 mL min^{-1}.

the presence of these chemical additives evidencing the efficient electron capture by these agents (Eq. (10)).

$$M^{n+} + e^{-}_{CB} \xrightarrow{h\nu} M^{(n-1)} \quad (10)$$

On the contrary, the addition of Ag^{+} shows a detrimental effect on the performance, being even worse than single WO_3. This behavior is probably caused because during irradiation Ag is deposited onto the surface of the catalyst, producing a darkening of the suspension and a permanent alteration of the semiconductor that affects negatively its photoactivity. On the other hand, in the literature it is reported that in homogeneous solutions with TiO_2 and Cu^{2+} a red colored material is formed on the surface of TiO_2 during irradiation which would correspond to metallic copper [36]. As in the experiment of WO_3/Cu^{2+}, no change in the coloration was observed. It can be said that the photogenerated electrons were consumed by Cu^{2+} ions to produce Cu^{+} instead of being reduced to Cu on WO_3.

Taylor and Noceti reported a yield of methanol of 54 μmol h^{-1} g^{-1} corresponding to La-doped WO_3 in the presence of MV^{2+} (electron transfer agent) [6], while in this study a yield of methanol of 55.5 μmol h^{-1} g^{-1} has been obtained with an undoped mesoporous WO_3 in the presence of Fe^{3+} (2 mM), which is a much less expensive chemical than methyl viologen. Therefore, the homogeneous reaction pathways involving Fe^{3+} and the peculiar properties of mesoporous materials can play an important role in heterogeneous systems for methane conversion.

The generation of ethane is also influenced by the electron scavenger or by the oxidant agent used (Fig. 5). A large difference in the production of ethane was found, following the increasing order $H_2O_2 > Fe^{3+} > Cu^{2+} > Ag$. In contrast to the other chemicals, the addition of H_2O_2 or Fe^{3+} (photolysis) leads to the formation of $HO^{\cdot}$ in the solution, as shown in Eqs. (11) and (12), respectively.

$$H_2O_2 + e^{-}_{CB} \rightarrow OH^{-} + HO^{\cdot} \quad (11)$$

$$Fe^{3+} + H_2O \xrightarrow{h\nu} Fe^{2+} + HO^{\cdot} + H^{+} \quad (12)$$

Based on the above, it seems clear that a higher formation of hydroxyl radicals in the aqueous medium promotes an increment of methyl radicals that stimulate the production of ethane (Eq. (13)), instead of generating CH_3OH. This result could reveal that the formation of methanol is predominantly favored by hydroxyl groups

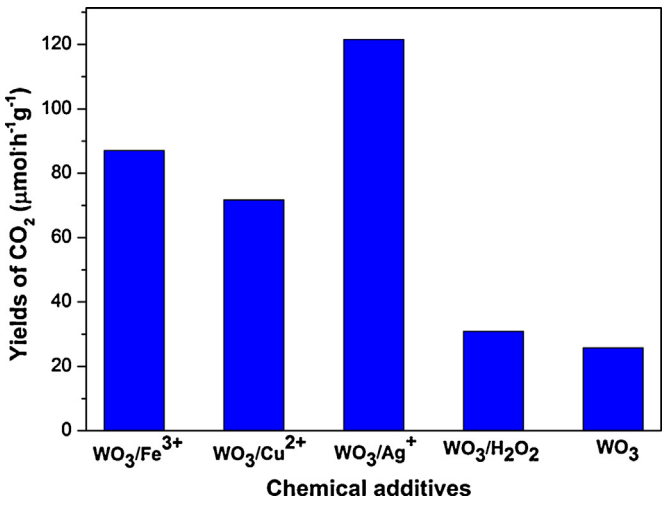

Fig. 6. Yields of CO_2 in the photocatalytic oxidation of CH_4 in systems of WO_3/Fe^{3+} (2 mM), WO_3/Cu^{2+} (0.1 mM), WO_3/Ag^+ (2 mM), WO_3/H_2O_2 (2 mM) and WO_3 at ~ 55 °C under UVC–visible light irradiation. WO_3 dosage is 1 g L^{-1}. Data corresponding to 2 h of irradiation in continuous methane flow of 4.5 mL min^{-1}.

and H_2O adsorbed on the surface of the catalyst and not by the addition of these radicals to the solution.

$$CH_3^{\bullet} + CH_3^{\bullet} \rightarrow C_2H_6 \quad (13)$$

This mechanism is in agreement with the results obtained with Cu^{2+} and Ag^+. Evidently, since these agents do not produce external hydroxyl radicals, the values of ethane were quite low. In the case of single WO_3, the recombination of charges is higher; therefore the amount of HO_{ads} and methanol produced is low and the ethane would come predominantly from HO•s generated directly by photolysis of water as described above.

Fig. 6 illustrates the CO_2 values resulting from the oxidation of organic products such as methanol and minor products, such as ethylene, ethanol and formaldehyde, during the photocatalytic process. In particular, the photooxidation in the presence of Ag^+ was drastic. The CO_2 generation rate with $AgNO_3$ was about 5 times higher than the rate of WO_3 in the absence of metal ions. Furthermore, it is interesting to notice that the addition of a free radical generator such as H_2O_2 does not increase CO_2 generation because these extra HO•'s generated are being consumed in the generation of methyl radicals.

As shown in Fig. 7, the conduction band potential of WO_3 is +0.09 V (vs. NHE, pH = 7) [37], while the standard redox potentials for Ag^+/Ag, Fe^{3+}/Fe^{2+} and Cu^{2+}/Cu^+ couples are 0.80, 0.77 and 0.16 V vs. NHE, respectively [38]. Then, by thermodynamic factors, the reduction of Ag^+ by the conduction band electrons of WO_3 is highly favorable. This clearly indicates that the rate of oxidation reactions involving holes is closely related to the effective charge separation by suitable electron scavengers. Therefore, WO_3/Ag^+ and WO_3/Fe^{3+} systems exhibit a higher oxidation than WO_3/Cu^{2+}. In the latter, the difference between the redox potential of Cu^{2+}/Cu^+ and the conduction band energy level is lower.

In general, the WO_3/Fe^{3+} system showed the largest rate of methanol. However, the CO_2 value is also high. In an effort to diminish the high photoactivity of this system that leads to the complete

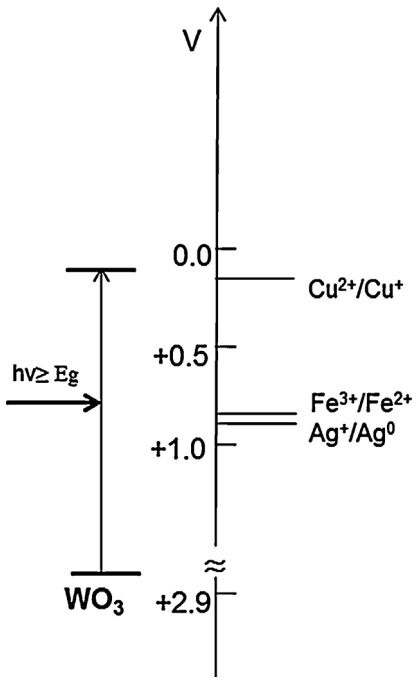

Fig. 7. Position of the conduction band edge and the valence band edge of WO_3 at pH = 7 and the standard redox potentials of the redox couples associated with the electron scavengers tested.

Table 2
Selectivity of the products in the photocatalytic oxidation of CH_4 on WO_3 catalyst in the presence of several chemical additives.

System	Selectivity (%)		
	CH_3OH	C_2H_6	CO_2
WO_3/Fe^{3+} (2 mM)	37.4	3.7	58.9
WO_3/Fe^{3+} (1 mM)	58.5	4.0	37.5
WO_3/Cu^{2+} (0.1 mM)	38.4	1.2	60.4
WO_3/Ag^+ (2 mM)	11.8	0.5	87.7
WO_3/H_2O_2 (2 mM)	34.3	11.2	54.5
WO_3	46.0	10.3	43.7

oxidation of organic compounds to CO_2, a lower concentration of Fe^{3+} (1 mM) was evaluated. The results are shown in Table 1. A decrease in the iron concentration results in an enhancement of photocatalytic performance of WO_3/Fe^{3+}; the CO_2 value was diminished by almost half in relation to Fe^{3+} (2 mM) and the yield of methanol was higher (67.5 μmol h^{-1} g^{-1}). Additionally, a control experiment with Fe^{3+} but without catalyst was performed under UVC-light irradiation. Compared with the blank experiment with water (no catalyst), the yield of methanol was increased, but it is much lower than the CH_3OH generated in the WO_3/Fe^{3+} system. Moreover, CO_2 increases 10-fold in relation to water (blank experiment). This result suggests that the presence of the catalyst is necessary to increase the selectivity to methanol.

Finally, Fig. 8 shows the productivity corresponding to each system. The addition of electron scavengers significantly increases the productivity, which is slightly larger for Fe^{3+} (2 mM) and Ag^+ systems. This fact evidences the need of capturing the generated

Table 1
Iron concentration, yield of CH_3OH, C_2H_6 and CO_2. WO_3 dosage is 1 g L^{-1}. Data corresponding to 2 h of irradiation in continuous methane flow of 4.5 mL min^{-1}.

System	Concentration	Yield of CH_3OH (μmol h^{-1} g^{-1})	Yield of C_2H_6 (μmol h^{-1} g^{-1})	Yield of CO_2 (μmol h^{-1} g^{-1})
WO_3/Fe^{3+}	2 mM	55.5	2.8	87.0
WO_3/Fe^{3+}	1 mM	67.5	2.3	43.3
WO_3	0 mM	27.1	2.9	25.8

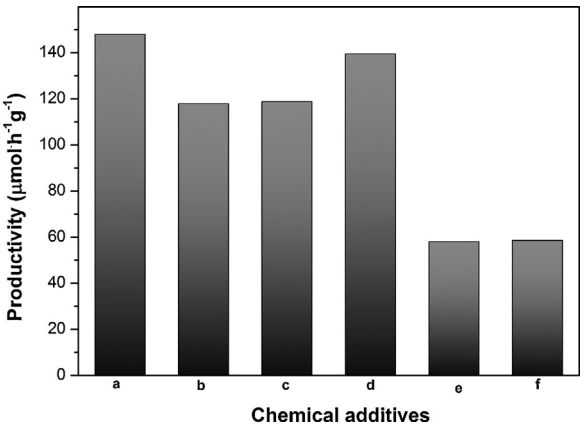

Fig. 8. Productivity corresponding to the following systems: (a) WO_3/Fe^{3+} (2 mM), (b) WO_3/Fe^{3+} (1 mM), (c) WO_3/Cu^{2+} (0.1 mM), (d) WO_3/Ag^{+} (2 mM), (e) WO_3/H_2O_2 (2 mM) and (f) WO_3 at ~ 55 °C under UVC–visible light irradiation. WO_3 dosage is 1 g L^{-1}. Data corresponding to 2 h of irradiation in continuous methane flow of 4.5 mL min^{-1}.

electrons in the WO_3 to enhance its photoactivity. However, as shown in Table 2, a higher productivity leads to a lower selectivity toward methanol, except in the case of Fe^{3+} (1 mM), which displayed a high productivity and the highest selectivity (over 58%) of formation of methanol.

4. Conclusions

The photocatalytic oxidation of CH_4 into CH_3OH over a mesoporous WO_3 using electron scavengers and H_2O_2 was examined. This study revealed that the photocatalytic activity of WO_3 toward methanol production could be enhanced by a factor of 2.5 and 1.7 by adding Fe^{3+} (1 mM) and Cu^{2+} (0.1 mM), respectively. The maximum CO_2 rate (36.5 μmol h^{-1}) was achieved for Ag^{+}, indicating that this metal ion is detrimental to the selective oxidation process. The formation of ethane was clearly favored by the addition of H_2O_2 and Fe^{3+} to the system. For instance, H_2O_2 reacts with electrons to form more hydroxyl radicals and Fe^{3+}, besides being reduced by e- in the conduction band of WO_3, can absorb UV light to generate $HO^{\bullet}$ and Fe^{2+}. The other chemicals (Cu^{2+} and Ag^{+}) only act as electron scavengers improving electron–hole pair separation that increase the formation of hydroxyl radicals on the surface of WO_3.

Acknowledgements

This work was partially supported by the European Regional Development Funds (ERDF, FEDER Programa Competitivitat de Catalunya 2007–2013), the Ministerio de Economia y Competitividad (CSD2009-00050) and the Framework 7 program under the project CEOPS (FP7-NMP-2012-309984).

Appendix A. Supplementary data

Supplementary data associated with this article can be found, in the online version, at http://dx.doi.org/10.1016/j.apcatb.2014.07.055.

References

[1] I. Karakurt, G. Aydin, K. Aydiner, Renew. Energ. 39 (2012) 40–48.
[2] M. Massa, R. Häggblad, S. Hansen, A. Andersson, Appl. Catal. A 408 (2011) 63–72.
[3] S. Lee, Methanol Synthesis Technology, CRC Press, Florida, 1990.
[4] G. Palmisano, E. García-López, G. Marcí, V. Loddo, S. Yurdakal, V. Augugliaro, L. Palmisano, Chem. Commun. 46 (2010) 7074–7089.
[5] M.A. Gondal, A. Hameed, Z.H. Yamani, A. Arfaj, Chem. Phys. Lett. 392 (2004) 372–377.
[6] C.E. Taylor, R.P. Noceti, Catal. Today 55 (2000) 259–267.
[7] M.A. Gondal, A. Hameed, A. Suwaiyan, Appl. Catal. A 243 (2003) 165–174.
[8] L. Li, M. Krissanasaeranee, S. Pattinson, M. Stefik, U. Wiesner, U. Steiner, D. Eder, Chem. Commun. 46 (2010) 7620–7622.
[9] L. Deng, X. Ding, D. Zeng, S. Tian, H. Li, C. Xie, Sensor. Actuat. B 163 (2012) 260–266.
[10] L.G. Teoh, Y.M. Hon, J. Shieh, W.H. Lai, M.H. Hon, Sensor. Actuat. B 96 (2003) 219–225.
[11] Y. Qin, F. Wang, W. Shen, M. Hu, J. Alloy. Compd. 540 (2012) 21–26.
[12] W. Zhenhai, W. Wei, L. Zhuang, Z. Hao, L. Jinghong, J. Chen, PCCP Phys. Chem. Ch. Ph. 15 (2013) 6773–6778.
[13] X. Yan, X. Zong, G. Qing, L. Wang, Prog. Nat. Sci. Mater. Int. 22 (2012) 654–660.
[14] Y. Usami, T. Hongo, A. Yamazaki, Micropor. Mesopor. Mater. 158 (2012) 13–18.
[15] E. Rossinyol, J. Arbiol, F. Peiró, A. Cornet, J.R. Morante, B. Tian, T. Bo, D. Zhao, Sensor. Actuat. B 109 (2005) 57–63.
[16] M. Litter, Appl. Catal. B 23 (1999) 89–114.
[17] P. Scherrer, Math-Phys. Klasse 2 (1918) 98–100.
[18] J. Tauc, A. Menth, J. Non-Cryst. Solids 8 (1972) 569–585.
[19] S. Songmei, W. Wenzhong, Z. Shaozhong, S. Meng, Z. Ling, J. Hazard. Mater. 178 (2010) 427–433.
[20] D. Sánchez-Martínez, A. Martínez-de la Cruz, E. López-Cuéllar, Mater. Res. Bull. 48 (2013) 691–697.
[21] C. Gómez-Solís, D. Sánchez-Martínez, I. Juárez-Ramírez, A. Martínez-de la Cruz, L.M. Torres-Martínez, J. Photochem. Photobiol. A Chem. 262 (2013) 28–33.
[22] G.W. Ho, K.J. Chua, D.R. Siow, Chem. Eng. J. 181 (2012) 181–182.
[23] C.E. Taylor, Catal. Today 84 (2003) 9–15.
[24] A.I. Gavrilyuk, Electrochim. Acta 44 (1999) 3027–3037.
[25] Y. Shen, R. Huang, Y. Cao, P. Wang, Mater. Sci. Eng. B 172 (2010) 237–241.
[26] C.D. Baertsch, S.L. Soled, E. Iglesia, J. Phys. Chem. B 105 (2001) 1320–1330.
[27] A. Tocchetto, A. Glisenti, Langmuir 16 (2000) 6173–6182.
[28] G. Ramis, G. Busca, C.L. Lietti, P. Forzatti, F. Bregani, Langmuir 8 (1992) 1744–1749.
[29] T. Ohtsuka, N. Goto, N. Sato, J. Electroanal. Chem. Interfacial Electrochem. 287 (1990) 249–264.
[30] A. Rougier, F. Portemer, A. Quédé, M.E. Marssi, Appl. Surf. Sci. 153 (1999) 1–9.
[31] G.D. Papakonstantinou, J.M. Jaksic, D. Labou, A. Siokou, M.M. Jaksic, Adv. Phys. Chem. 2011 (2011) 22.
[32] C. Bechinger, G. Oefinger, S. Herminghaus, P. Leiderer, J. Appl. Phys. 74 (1993) 4527–4533.
[33] U.O. Krašovec, A.S. Vuk, B. Orel, Electrochim. Acta 46 (2001) 1921–1929.
[34] M.J. Sienko, H. Oesterreicher, J. Am. Chem. Soc. 90 (1968) 6568–6570.
[35] J. Pfeifer, C. Guifang, P. Tekula-Buxbaum, B.A. Kiss, M. Farkas-Jahnke, K. Vadasdi, J. Solid State Chem. 119 (1995) 90–97.
[36] T. Arai, M. Yanagida, Y. Konishi, A. Ikura, Appl. Catal. B 84 (2008) 42–47.
[37] K. Sayama, K. Mukasa, R. Abe, Y. Abe, H. Arakawa, J. Photochem. Photobiol. A Chem. 148 (2002) 71–77.
[38] A.J. Bard, R. Parsons, J. Jordan, Standard Potentials in Aqueous Solution, Marcel Dekker, New York, 1985.